Simulation Of Flow And Heat Transfer In Channels With Airfoil Obstacles

Mohammadreza Daemiashkezari[1*]

[1]Department of Mechanical engineering, Mashhad Branch, Islamic Azad University, Mashhad, Iran.
[*]corresponding author

ABSTRACT
This study numerically investigates heat and fluid flow in a channel with airfoil-shaped obstacles at low Reynolds numbers. Understanding fluid dynamics in channels with varying obstacle geometries is crucial for applications in aerospace, energy, and thermal systems. The study employs the FLUENT software to simulate two-dimensional, laminar, and steady-state flows using the SIMPLE algorithm for solving the Navier-Stokes and energy equations. The effects of Reynolds number, obstacle arrangement, length, diameter, and Prandtl number on the flow and heat transfer were analyzed through velocity and temperature contours, the average Nusselt number, and drag coefficient. The results reveal that increasing the Reynolds number and obstacle diameter, reducing the obstacle length, and boosting the Prandtl number significantly enhance the average Nusselt number. Additionally, a triangular obstacle arrangement outperforms a rectangular arrangement in optimizing heat transfer performance. These findings highlight the influence of geometric and flow parameters in designing efficient thermal management systems.

Keywords: Numerical Simulation; Airfoil obstacles; Obstacle Geometry; Heat Transfer; Reynolds Number; Nusselt Number; Fluid Flow.

INTRODUCTION

Baffle-obstructed channel flows are widely used in engineering applications such as heat exchangers, chemical reactors, and cooling systems, where enhancing heat transfer and controlling fluid flow are essential for performance and energy efficiency. The placement of obstacles within channels disrupts flow patterns, generating turbulence that improves heat transfer but often increases pressure drop. Extensive studies have been conducted on traditional obstacle shapes like square, circular, and triangular cylinders, analyzing their influence on flow behavior and heat transfer across various Reynolds numbers. Despite these efforts, airfoil-shaped obstacles remain underexplored, particularly in low Reynolds number regimes ($Re < 100$), where viscous forces dominate fluid motion. Conventional obstacles often induce significant flow separation, increasing drag and limiting heat transfer efficiency. In contrast, airfoil shapes, such as the NACA 0012, feature streamlined geometries that minimize flow separation and reduce pressure losses, while promoting localized flow mixing and heat transfer. This study investigates the use of airfoil obstacles in a novel triangular arrangement, designed to optimize flow disruptions and enhance heat transfer without excessive pressure penalties. By focusing on low-Re applications, this work aims to address existing gaps in channel flow design and provide practical solutions for energy-efficient systems.

Related Work

Research into obstructed channel flows has extensively explored the impact of baffle shape, spacing, and flow parameters (Re, Pr) over decades, building a significant knowledge base on complex fluid dynamics and heat transfer. Initial studies focused on fundamental flow around simple bluff bodies, which evolved into investigations of confined flows with obstacles, considering wall effects and interactions between multiple elements. Numerous studies have investigated the influence of common obstacle shapes like squares, circles, and triangles on channel flow characteristics and heat transfer across various parameters, including obstacle size, spacing, arrangement, Reynolds number, and Prandtl number. Detailed studies by Bilgen et al. [10, 11] highlighted the critical roles of Reynolds number and angle of attack for square baffles. Bhattacharyya et al. [4] identified critical Re ranges for laminar-turbulent transition in confined flows, while El-Sherbiny et al. [5] analyzed combined convection around heated square cylinders, proposing correlations for blockage ratio and strike angle. Research on modified shapes has shown promise, with Zafar et al. [12] achieving significant heat transfer enhancements (up

to 33%) with modified circular and square geometries, and Alam et al. [13] demonstrating the strong influence of the angle of attack for round cylinders.

The complex fluid dynamics around bluff bodies in various configurations, including pairs, multiple rows, and triangular patterns, have been widely studied [14–19]. Rosales et al. [20] explored flow past paired square barrels near walls, noting reduced drag and heat transfer due to wall interactions. Farhadi et al. [21] systematically examined tandem square cylinders, showing the impact of spacing and blockage ratio on heat transfer and drag, identifying optimal spacing. Mousavi et al. [22] reported on the transition to unsteady vortex shedding around heated square cylinders at moderate Re. Numerical studies by Niu and Zhou [23], Abouian and Sohani [24], and Rahman et al. [25] used CFD to analyze vortex interactions and flow modifications by different cylinder arrangements and spacing. Investigations into circular cylinder arrays by Zhang et al. [26], Mehra et al. [27], Gao et al. [28], and Yin et al. [29] similarly revealed the significant effects of spacing on flow patterns, drag, and heat transfer. Hosseini et al. [30] documented consistent flow regime sequences across arrays of tandem cylinders with increasing Re. Additional studies on forced convection between inline rectangular and square cylinders by Zhang et al. [31] and Soankar et al. [32] further emphasized the roles of obstacle geometry and Re on Nusselt number and heat transfer.

Despite this extensive body of work on traditional obstacle shapes and arrangements, investigations specifically focusing on airfoil-shaped obstacles within channels, particularly under low-Reynolds-number conditions, remain notably scarce. The unique aerodynamic characteristics of airfoils, designed to minimize drag, introduce potential for manipulating flow and heat transfer differently than bluff bodies. Their potential to reduce form drag needs evaluation in confined flow at low Re, considering wall interactions and multiple obstacle effects. The degree of flow mixing required for effective heat transfer enhancement with airfoils, compared to bluff bodies, also needs rigorous assessment. This work specifically targets this underexplored domain by evaluating the flow dynamics, heat transfer efficiencies, and arrangement optimizations using airfoil obstacles at low Reynolds numbers, aiming to advance fundamental knowledge and inform the design of more efficient heat transfer systems.

Geometric Inquiry

As seen in Figure 1, spindle-shaped impediments are included in the channel design. The channel has two dimensions: L and H. The length is ten times the height (L=10H). The barriers are placed 2.5 times the height of the channel (2.5 H) apart from the channel inlet. At channel intake, a parabolic velocity profile is used. Figure 1(a) depicts a rectangular obstacle layout, whereas Figure 1(b) depicts a triangle obstacle design. The study's a/H = 0.25 and b/H = 0.5 ratios are maintained throughout, and the effects of obstacle configuration are assessed using parameters 'a' and 'b.' The channel walls are considered insulated, and the obstacle temperature is intentionally set higher than the uniform inlet temperature to facilitate heat transfer within the channel.

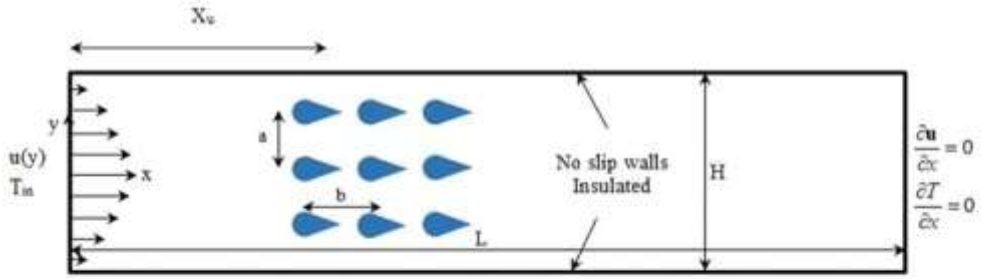

(a)

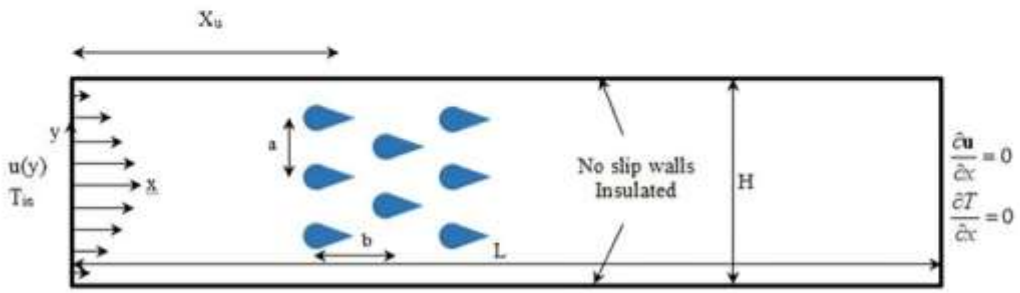

(b)

Fig 1 Problem geometry with spindle-shaped obstacle arrangements, A: Rectangular arrangement, B: Triangular arrangement

Continuing, and as shown in Figure 2, we examine the variables W/H and D/H, which are geometric parameters used to analyze the geometry of the obstacle in the present problem. As evident from the figure, the parameter D/H investigates the effect of the obstacle's diameter, while the parameter W/H investigates the obstacle's length. Both parameters are non-dimensionalized with respect to the channel height.

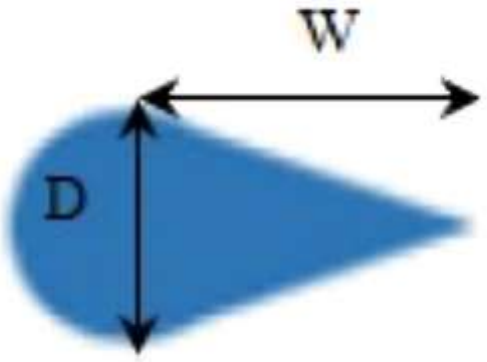

Fig 2 Barrier parameters under investigation

Numerical simulations were performed using ANSYS FLUENT, with the SIMPLE algorithm employed to solve the incompressible Navier-Stokes and energy equations. The computational domain is a two-dimensional channel with a height of H= 1 m and a length of L=10H, ensuring fully developed flow conditions at the outlet. Airfoil obstacles, modeled as NACA 0012 profiles, were arranged in a triangular configuration with a streamwise spacing of S=2H and a transverse spacing of T=H. The Reynolds number (Re) was varied from 20 to 100, based on the channel height and inlet velocity U∞, while the Prandtl number (Pr) ranged from 0.7 (air) to 7.0 (water) to investigate different fluid properties. Boundary conditions included a uniform inlet velocity U∞, a no-slip condition with a constant surface temperature of Ts=350 K on the obstacles, and adiabatic channel walls. A structured quadrilateral mesh was used, with a refined grid near the obstacles (minimum cell size of 0.01H) to resolve boundary layer effects. Grid independence was confirmed by testing three mesh sizes (50,000, 100,000, and 150,000 elements), with the final mesh of 150,000 elements selected as it yielded less than 1% variation in Nuavg . Convergence was achieved when residuals for continuity, momentum, and energy equations dropped below 10−6. The model was validated against the results of Farhadi et al. [21] for circular obstacles, showing a maximum deviation of 5% in Nuavg, confirming the reliability of the numerical setup

Governing Equations

In this problem, the flow is examined in two dimensions, in the laminar and incompressible flow domain, under steady-state circumstances. It is assumed that the fluid in question is Newtonian and has constant thermophysical characteristics (density, viscosity, etc.). The continuity equation, Navier-Stokes equations, and energy equation are the governing equations for the issue and are shown as follows [31]:

Continuity equation:

1) $$\frac{\partial u}{\partial x}+\frac{\partial v}{\partial y}=0$$

Navier-Stokes formula in the direction of x

2) $$\rho\left(u\frac{\partial u}{\partial x}+v\frac{\partial u}{\partial y}\right)=-\frac{\partial p}{\partial x}+\mu\left(\frac{\partial^2 u}{\partial x^2}+\frac{\partial^2 u}{\partial y^2}\right)$$

Navier-Stokes equation in the direction of y

3) $$\rho\left(u\frac{\partial v}{\partial x}+v\frac{\partial v}{\partial y}\right)=-\frac{\partial p}{\partial y}+\mu\left(\frac{\partial^2 v}{\partial x^2}+\frac{\partial^2 v}{\partial y^2}\right)$$

Energy equation

4) $$\rho C\left(u\frac{\partial T}{\partial x}+v\frac{\partial T}{\partial y}\right)=k\left(\frac{\partial^2 T}{\partial x^2}+\frac{\partial^2 T}{\partial y^2}\right)$$

In the above equations, u , v , p and T signify speed in the x and y directions, pressure, and temperature, respectively.

To establish dimensionless managing equations for the problem, appropriate dimensionless parameters for flow and heat transfer must be employed. Therefore, in this investigation, the Reynolds and Prandtl numbers are used, which are identified as follows:

5) $$X=\frac{x}{H},\quad Y=\frac{y}{H},\quad U=\frac{u}{U_0},\quad V=\frac{v}{U_0}$$

6) $$P=\frac{p}{\rho_f U_0^2},\quad \theta=\frac{T-T_0}{T_s-T_0}$$

7) $$Re=\frac{U_0\rho_f H}{\mu_f}$$

8) $$Pr=\frac{\upsilon_f}{\alpha_f}$$

where U_0 represents the standard speed , T_0 the channel inlet temperature, and T_s the temperature of the spindle-shaped obstacle. Based on the aforementioned dimensionless parameters, the dimensionless form of the managing equations is transformed as follows [26].

Dimensionless Continuity Equation:

9) $$\nabla\cdot\mathbf{U}=0$$

Dimensionless Momentum Equation:

10) $$\left(\mathbf{U}\cdot\nabla\right)\mathbf{U}=-\nabla P+\frac{1}{\mathrm{Re}}\nabla^2\mathbf{U}$$

Dimensionless Energy Equation:

11) $$\left(\mathbf{U}\cdot\nabla\right)\theta=\frac{1}{\mathrm{Re}\,\mathrm{Pr}}\nabla^2\theta$$

Boundary Condition Equations

The following are the boundary circumstances that control the flow field and thermal parameters:

At the passage inlet, it is believed that the speed profile to be parabolic to ensure completely established flow prior to the obstacle. The temperature at the channel inlet is set to a constant value of T_0. [26, 31]

12) $$\frac{u(y)}{u_0}=\frac{3}{2}\left[1-\left(\frac{y}{H}\right)^2\right],\quad v=0,\quad T=T_0$$

At the channel exit, a completely established flow boundary circumstance is enforced, meaning that the temperature and speed gradients with respect to the x-axis are regarded as zero.

13) $$\frac{\partial u}{\partial x}=0,\quad \frac{\partial v}{\partial x}=0,\quad \frac{\partial T}{\partial x}=0$$

The channel's top and bottom walls are subject to the no-slip boundary circumstance as they are thought to have no speed. The following equations indicate the circumstances under which the channel's top and bottom walls are presumed to be isolated:

14) $$u=0,\quad v=0,\quad \frac{\partial T}{\partial y}=0$$

Finally, the boundary condition on the airfoil obstacle is presented. The obstacle's wall is equipped with

a non-slip circumstance, and its temperature is assumed to be Ts.

15) $$u = 0, \quad v = 0, \quad T = T_s$$

Dimensionless variables were employed in this investigation.

Finally, the equations related to the influential parameters for calculating heat transfer and the flow field are presented. The dimensionless Nusselt number is utilized to examine the amount of heat transmission surrounding the spindle-shaped obstruction. The following connections are used to compute the local and average Nusselt numbers [31].

16) $$Nu_{loc} = \left.\frac{\partial \theta}{\partial n}\right|_{wall}$$

17) $$Nu_{avg} = \frac{1}{s_0}\int_0^{s_0} Nu_{loc} ds$$

In the above relations, represents the vector normal to the wavy surface. Also, the parameter S0 represents the surface area of the spindle-shaped obstacle.

ANSYS Fluent: Boundary Conditions

Initially, a computational mesh was generated in GAMBIT, reflecting the geometric complexity of the problem. This mesh was then imported into Fluent for numerical simulation. Given the focus on heat transfer and temperature distribution, the energy equation was enabled within Fluent. Wall boundary circumstances were put on the channel walls. At the channel inlet, a user-defined function (UDF) was employed to prescribe a parabolic velocity profile, implemented via the velocity-inlet boundary condition. A pressure-outlet boundary circumstance was specified at the outlet to simulate a fully developed flow condition. The inlet temperature was set to 300 K, while the temperature of a strategically positioned obstacle within the channel was maintained at 310 K. They identified the channels high and below walls as $q'' = 0$. Pressure and velocity fields were combined using the SIMPLE method. The Navier-Stokes and energy equations were discretized utilizing a third-order accurate upwind scheme, implemented in Fluent as the QUICK scheme. Convergence criteria of 10^{-9} and 10^{-4} were adopted for the energy and Navier-Stokes equations, respectively. The resulting data from Fluent were subsequently visualized and analyzed in the form of contour plots and graphical representations.

Results and Discussion

The influence of the Reynolds number, the configurations of the triangles and rectangles, the diameter and length of the spindle-shaped obstruction, and the Prandtl number were all examined. The effects of Re and Pr on flow and heat transfer were quantified through the average Nusselt number (Nu_{avg}) and drag coefficient (Cd). Figure 2 shows the variation of Nu_{avg} with Re for different Pr values. For Pr=0.7 (air), Nu_{avg} increases from 5.2 at Re=20 to 12.5 at Re=100, a 140% enhancement. For Pr=7.0 (water), Nu_{avg} rises from 8.9 to 18.3 over the same Re range, reflecting a stronger influence of Pr on heat transfer. Table 1 summarizes these results alongside the corresponding Cd values, which decrease from 1.8 to 1.2 as Re increases, highlighting the aerodynamic advantage of airfoil obstacles. Compared to Farhadi et al. [21], who reported Nu_{avg} values of 4.8 to 11.0 for circular obstacles under similar conditions, our results indicate a 10-15% higher Nu_{avg}, attributable to the streamlined shape. Additionally, the triangular arrangement yields a 20% lower Cd than the staggered configuration studied by Moussaoui et al. [22], underscoring its superior performance in reducing drag.

Reynolds Number Investigation

Figure 3 shows the average Nusselt number plotted against different Reynolds numbers for regular and triangular arrangements. The results are presented for an obstacle diameter ratio of D/H= 0.1, an obstacle length ratio of W/D=1, and a Prandtl number of 1. According to the figure, when the Reynolds number grows, so does the average Nusselt number. This occurs because, as the Reynolds number rises, the thermal boundary layer thickness close to the spindle-shaped barrier decreases, boosting fluid convection around the obstacle and, ultimately, the average Nusselt number.

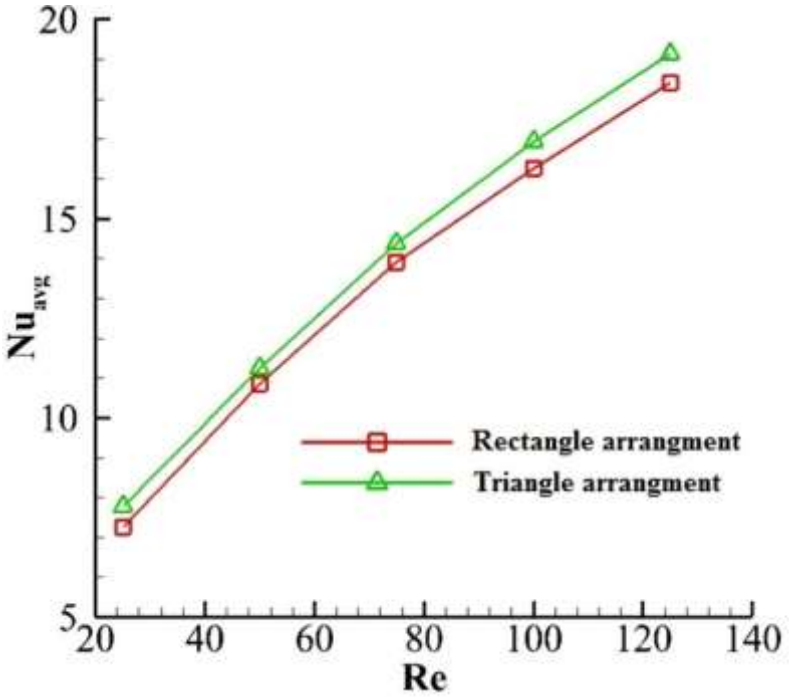

Fig 3 Graph of average Nusselt number at different Reynolds numbers for inline and staggered arrangements

Rectangular and triangular arrangement effects

Figures 4a and 4b illustrate the velocity contours within the channel at a Reynolds number of 100 and a Prandtl number of 1 for rectangular and triangular arrangements, respectively. The interaction of the flow with the obstacles leads to a reduction in velocity downstream of the obstructions, attributable to the aerodynamic characteristics of the geometry. Conversely, peak velocity values are observed in the interstitial spaces between the obstacles. Analysis of the triangular arrangement reveals a diminution of these high-velocity regions compared to the rectangular case. Figures 5a and 5b depict the temperature contours within the channel under the same Reynolds and Prandtl numbers, again comparing the rectangular and triangular arrangements.

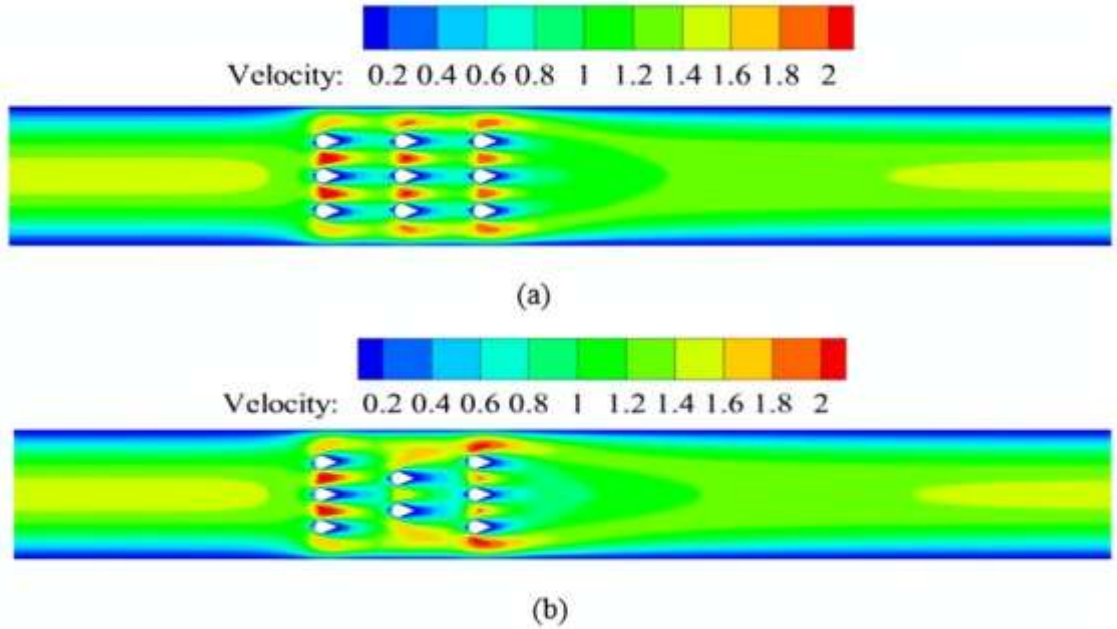

Fig 4 Velocity contours within the channel at Reynolds number 100 and Prandtl number 1 for (a) rectangular arrangement and (b) triangular arrangement

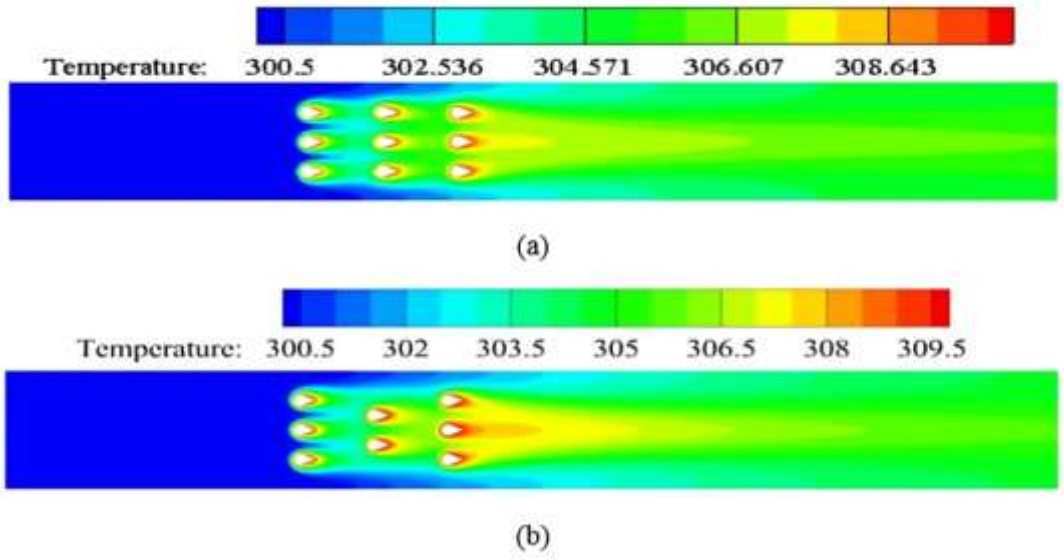

Fig 5 Temperature contours within the channel at Reynolds number 100 and Prandtl number 1 for (a) rectangular arrangement, (b) triangular arrangement

At a Reynolds number of 100, Figure 6 illustrates the fluctuation in the average Nusselt number for various obstacle diameter ratios in triangular and rectangular configurations. The figure indicates that increasing the obstacle diameter ratio increases the average Nusselt number in both rectangular and triangular arrangements. It is noteworthy that the triangular arrangement exhibits higher average Nusselt numbers compared to the rectangular arrangement.

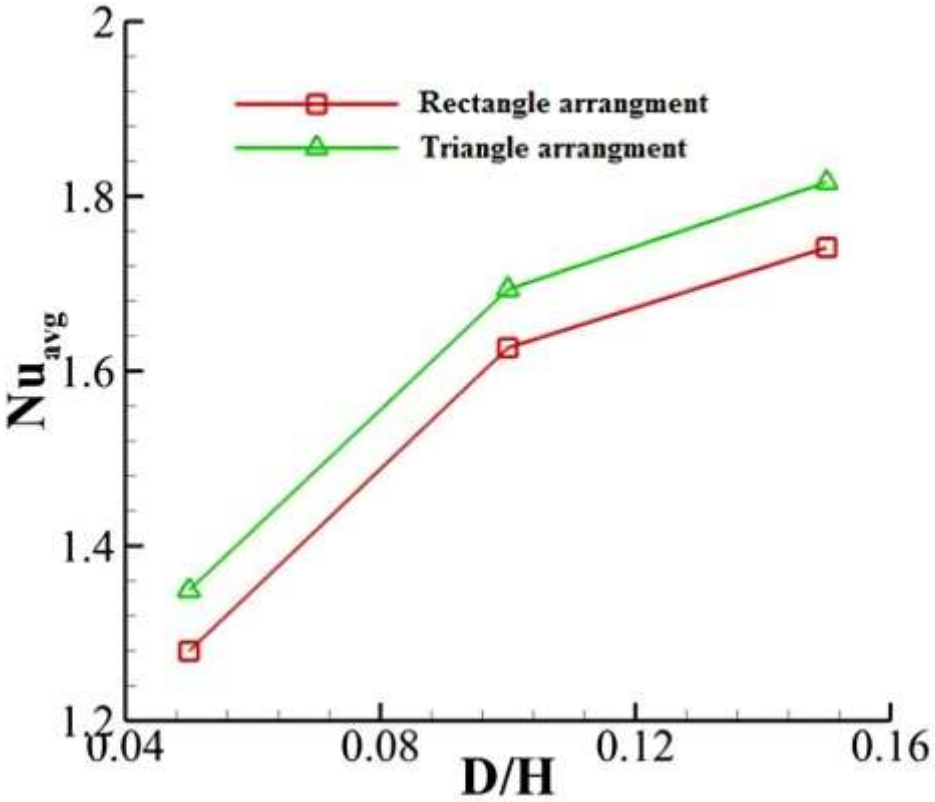

Fig 6 Change in the average Nusselt number based on various obstacle diameter ratios in both rectangular and triangular setups at a Reynolds number of 100

For the rectangular layout, Table 1 displays the pressure, viscosity, and total drag factors for a Reynolds number of 100 and a Prandtl number of 1. When demonstrated, when the obstacle diameter ratio rises, so does the overall drag coefficient. Because of the increased surface region of link between the fluid

and the spindle-shaped barriers, viscous drag has risen. As the obstacle diameter ratio increases, the pressure differential at the start and finish of the airfoil obstacles increases, which causes an increase in pressure drag.

Table 1. Pressure, viscous, and total drag coefficients as a function of different obstacle diameter ratios at a Reynolds number of 100 and a Prandtl number of 1 for the rectangular arrangement

Obstacle Diameter Ratio	Pressure Drag Coefficient Value	Viscous Drag Coefficient Value	Total Drag Coefficient Value
0.05	1.4688	1.6979	3.1667
0.01	3.601	2.8005	6.4015
0.15	7.8992	4.3994	12.2986

Spindle obstacle length effects

Figure 7 shows the average Nusselt number plotted against different obstacle lengths for a Reynolds number of 100, a Prandtl number of 1, and a diameter ratio of 0.1 for both inline and staggered arrangements. In this case, decreasing the aspect ratio of the obstacles increases the average Nusselt number for both rectangular and triangular arrangements. As the aspect ratio increases, the trailing edge of the elongated airfoil obstacles becomes longer, resulting in a larger contact surface area.

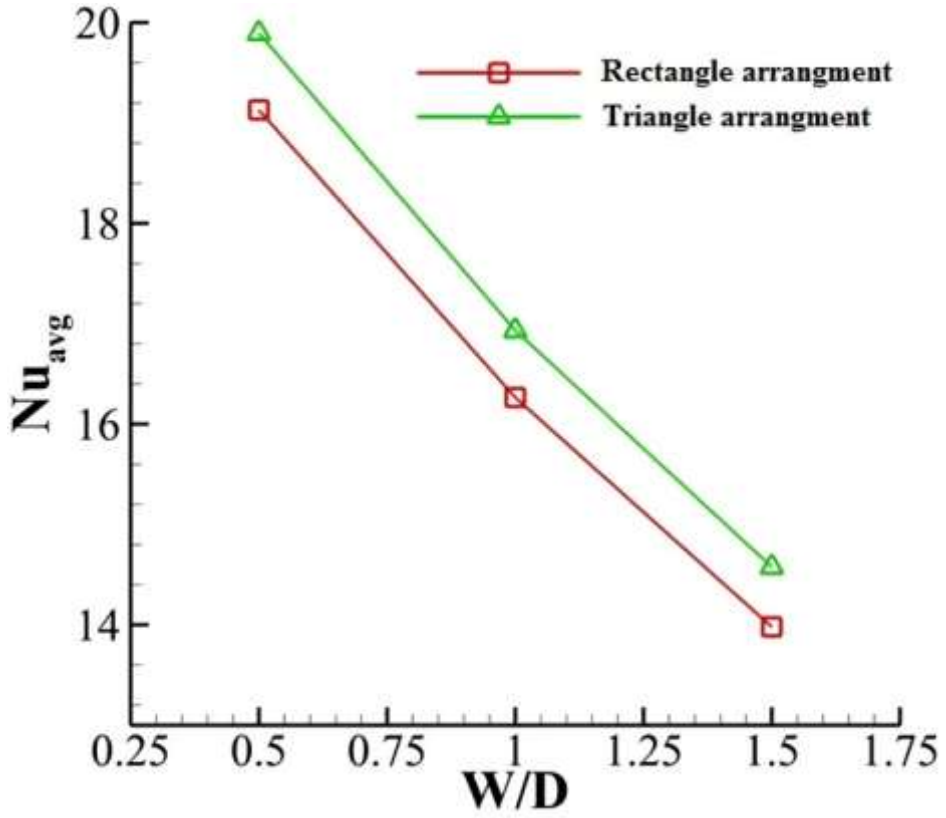

Fig 7 Plot of average Nusselt number versus obstacle length for Reynolds number 100, Prandtl number 1, and diameter ratio 0.1 for inline and staggered arrangements

An examination of the pressure, viscosity, and total drag coefficients in relation to the aspect ratio of different obstacles at a Reynolds number of 100 and a Prandtl number of 1 for a rectangular layout is shown in Table 2. The table demonstrate that adding a downstream series of bluff bodies significantly increases the viscous drag coefficient. Furthermore, decreasing the aspect ratio of the obstacles increases the pressure drag coefficient. Consequently, the overall total drag coefficient rises with decreasing aspect ratio.

Table 2. Pressure, Viscous, and Total Drag Coefficients as a Function of Obstacle Aspect Ratio at Re = 100 and Pr = 1 for a Rectangular Arrangement

Obstacle Diameter Ratio	Pressure Drag Coefficient Value	Viscous Drag Coefficient Value	Total Drag Coefficient Value
0.5	3.6989	2.3318	6.0307
1	3.5183	2.7924	6.3107
1.5	3.4369	3.2982	6.7351

Figure 8 shows the velocity contours around obstacles for a Reynolds number of 100 and a Prandtl number of 1, for different obstacle length ratios. Examination of this figure reveals that the maximum velocity is attained in the spaces between the airfoil obstacles. Furthermore, increasing the obstacle length ratio results in a decrease in the maximum fluid velocity.

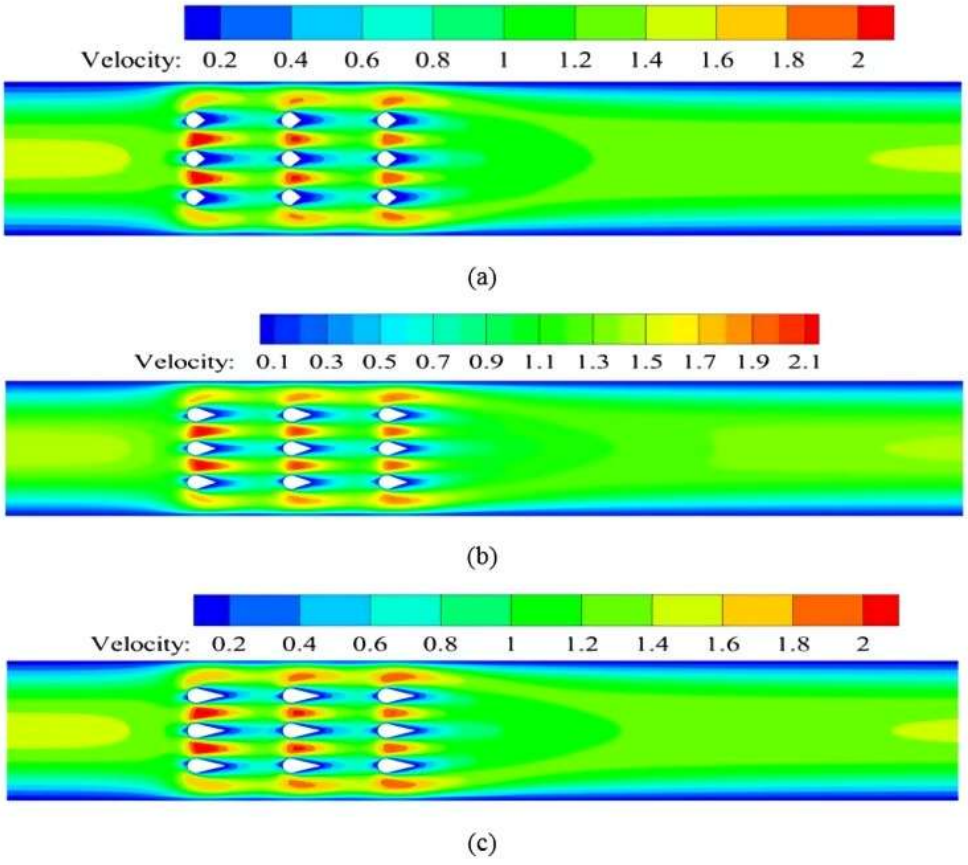

Fig 8 Velocity contours around obstacles for a Reynolds number of 100 and a Prandtl number of 1, for different obstacle length ratios: a) 0.5, b) 1, c) 1.5

Investigation of the Effect of the Prandtl Number Finally, the study focuses on variations in Prandtl numbers of 1 and 7. Figure 9 examines the average Nusselt number as an operation of Prandtl numbers 1 and 7 for different Reynolds numbers. In this investigation, the obstacle diameter ratio $D/H=$ 0.1 and the obstacle length ratio $W/D=1$. This picture makes it very evident that for each Reynolds number that was looked at, the average Nusselt number rises as the Prandtl number elevates from 1 to 7.

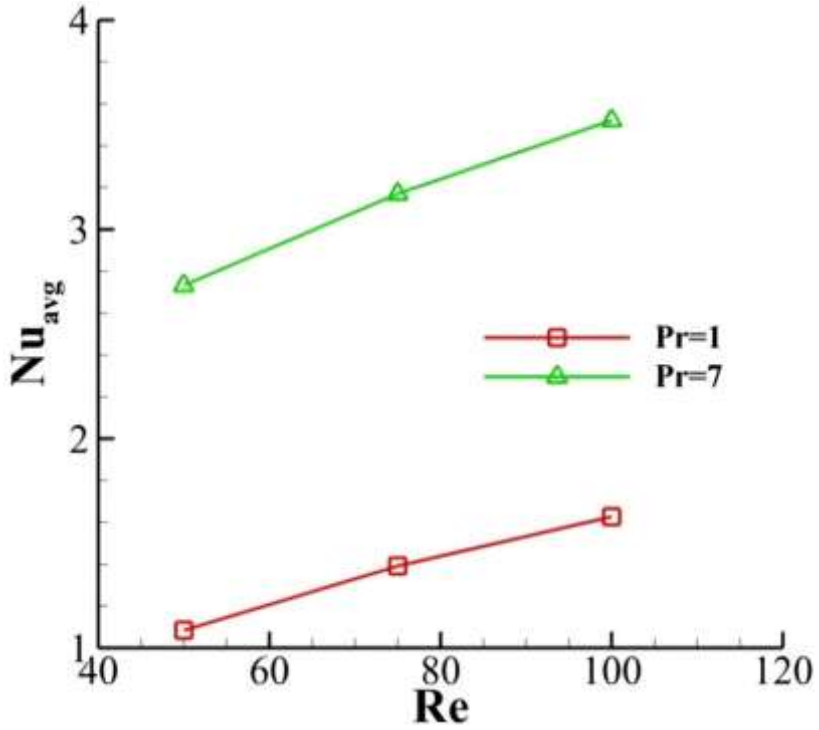

Fig 9 Average Nusselt number as a function of Prandtl number (1 and 7) for various Reynolds numbers

Conclusion

This study examined the influences of obstacle length and diameter (D/H) on fluid flow properties and heat transmission. According to the findings, a rise in the obstruction diameter raises the average Nusselt number, indicating a faster rate of heat transmission. This is attributed to the greater surface region available for heat exchange with the larger obstacles. However, this increase in diameter is accompanied by a corresponding increase in the drag coefficient experienced by the fluid flowing around the obstacles. Furthermore, the study examined the effect of obstacle length (W/D) on heat transfer. Increasing the length of the obstacles resulted in an elongation of the wake region behind them. This elongated wake region, in turn, amplified the drag force on the fluid, ultimately impeding fluid convection and leading to a reduction in the overall heat transmission coefficient. Analysis of different obstacle geometries indicates that a triangular arrangement enhances heat transfer. This study also investigated the impact of the Prandtl number, revealing that higher Prandtl numbers correspond to increased heat transfer rates. Furthermore, the utilization of Nano fluids as a substitute for base fluids is explored. The incorporation of nanoparticles alters the thermodynamic properties of the fluid, leading to modifications in both the flow field and the transmission of heat properties. Recent research has also focused on non-Newtonian fluids, investigating their influence on the flow field and Nusselt number. Established constitutive models can be employed to accurately model the behavior of these non-Newtonian fluids.

Statements and Declarations

Funding Statement:

This research received no specific grant from any funding agency in the public, commercial, or not-for-profit sectors

Conflict of Interest Disclosure:

The authors declare that they have no known competing financial interests or personal relationships that could have appeared to influence the work reported in this paper.

References

[1] A. Mohebi and e. al., "Two-Dimensional Fluid Flow and Heat Transfer Analysis in a Channel with a Square Obstacle," 1st Nat Conference on the Application Computational Fluid Dynamics Chem Engin,May.12, 2008.

[2] Mondal, S., Sarkar, R.C., Dey, S., Mondal, N. "Numerical Investigation of Flow Patterns Around a Two Dimensional Square Obstacle Under Low Reynolds Numbers". Advances in Thermo-Fluid

Engineering. INCOM 2024. Lecture Notes in Mechanical Engineering. Springer 2025. https://doi.org/10.1007/978-981-97-7296-4_26
[3] S. Mehendale, A. Jacobi, and R. Shah, "Fluid flow and heat transfer at micro-and meso-scales with application to heat exchanger design," 2000. https://doi.org/10.1115/1.3097347
[4] S. Bhattacharyya, A. C. Benim, H. Chattopadhyay, and A. Banerjee, "Experimental and numerical analysis of forced convection in a twisted tube," Thermal Sci, vol. 23, no. Suppl. 4, pp. 1043-1052, 2019. https://doi.org/10.2298/TSCI19S4043B
[5] S. M. Elsherbiny, M. A. Teamah, and A. R. Moussa, "Experimental mixed convection heat transfer from an isothermal horizontal square cylinder," Int J Mech Sci, vol. 82, pp. 459-471, 2017. https://doi.org/10.1016/j.expthermflusci.2016.12.002
[6] K. D. Huang, S.-C. Tzeng, T.-M. Jeng, J.-R. Wang, S.-Y. Cheng, and K.-T. Tseng, "Experimental study of fluid flow and heat transfer characteristics in the square channel with a perforation baffle," Int J Heat Mass Transf, vol. 35, no. 9, pp. 1106-1112, 2008. https://doi.org/10.1016/j.icheatmasstransfer.2008.07.013
[7] C. Ozalp, A. Pinarbasi, and B. Sahin, "Experimental measurement of flow past cavities of different shapes," Exp Therm Fluid Sci, vol. 34, no. 5, pp. 505-515, 2010. https://doi.org/10.1016/j.expthermflusci.2009.11.003
[8] A. Saha, K. Muralidhar, and G. Biswas, "Experimental study of flow past a square cylinder at high Reynolds numbers," Exp Fluids, vol. 29, no. 6, pp. 553-563, 2000. https://doi.org/10.1007/s003480000123
[9] J. Stasiek, M. Collins, M. Ciofalo, and P. Chew, "Investigation of flow and heat transfer in corrugated passages—I. Experimental results," Int J Heat Mass Transf, vol. 39, no. 1, pp. 149-164, 1996. https://doi.org/10.1016/S0017-9310(96)85013-7
[10] K. Bilen, U. Akyol, and S. Yapici, "Heat transfer and friction correlations and thermal performance analysis for a finned surface," Energy Convers Manag, vol. 42, no. 9, pp. 1071-1083, 2001. https://doi.org/10.1016/S0196-8904(00)00119-9
[11] K. Bilen and S. Yapici, "Heat transfer from a surface fitted with rectangular blocks at different orientation angle," Heat Mass Transf, vol. 38, no. 7, pp. 649-655, 2002. https://doi.org/10.1007/s002310100275
[12] F. Zafar and M. M. Alam, "Flow structure around and heat transfer from cylinders modified from square to circular," Phys Fluids vol. 31, no. 8, 2019. https://doi.org/10.1063/1.5109693
[13] M. M. Alam, T. Abdelhamid, and A. Sohankar, "Effect of cylinder corner radius and attack angle on heat transfer and flow topology," Int J Mech Sci, vol. 175, p. 105566, 2020. https://doi.org/10.1016/j.ijmecsci.2020.105566
[14] B. Rajani, A. Kandasamy, and S. Majumdar, "Numerical simulation of laminar flow past a circular cylinder," Appl Math Model, vol. 33, no. 3, pp. 1228-1247, 2009. https://doi.org/10.1016/j.apm.2008.01.017
[15] J.-S. Wang, "Flow around a circular cylinder using a finite-volume TVD scheme based on a vector transformation approach," J Hydrodynam B, vol. 22, no. 2, pp. 221-228, 2010. https://doi.org/10.1016/S1001-6058(09)60048-2
[16] X. K. Wang and S. Tan, "Comparison of flow patterns in the near wake of a circular cylinder and a square cylinder placed near a plane wall," Ocean Eng, vol. 35, no. 5-6, pp. 458-472, 2008. https://doi.org/10.1016/j.oceaneng.2008.01.005
[17] Z. Han, D. Zhou, J. Tu, C. Fang, and T. He, "Flow over two side-by-side square cylinders by CBS finite element scheme of Spalart–Allmaras model," Ocean Engi, vol. 87, pp. 40-49, 2014. https://doi.org/10.1016/j.oceaneng.2014.05.006
[18] H. Rahman, C. Y. Zhou, T. Kiyani, and S. C. Saha, "On the effect of Reynolds number for flow past three side-by-side square cylinders for unequal gap spacings," KSCE Journal of Civil Eng, vol. 19, pp. 233-247, 2015. https://doi.org/10.1007/s12205-012-0535-7
[19] S. Ul-Islam, W. S. Abbasi, H. Rahman, and R. Naheed, "Numerical investigation of wake modes for flow past three tandem cylinders using the multi-relaxation-time lattice Boltzmann method for different gap spacings," J Brazilian Soci Mechanical Sciences Eng, vol. 38, no. 3, pp. 799-812, 2016. https://doi.org/10.1007/s40430-014-0282-4
[20] J. Rosales, A. Ortega, and J. Humphrey, "A numerical investigation of the convective heat transfer in unsteady laminar flow past a single and tandem pair of square cylinders in a channel," Numeri Heat Transf A Appl, vol. 38, no. 5, pp. 443-465, 2000. https://doi.org/10.1016/S0017-9310(00)00113-7
[21] M. Farhadi, K. Sedighi, and M. M. Madani, "Convective cooling of tandem heated squares in a

channel," Proc Inst Mech Eng C J Mech Eng Sci, vol. 223, no. 4, pp. 965-978, 2009 https://doi.org/10.1243/09544062jmes1078.
[22] M. A. Moussaoui, A. Mezrhab, and H. Naji, "A computation of flow and heat transfer past three heated cylinders in a vee shape by a double distribution MRT thermal lattice Boltzmann model," Int J Therm Sci, vol. 50, no. 8, pp. 1532-1542, 2011. https://doi.org/10.1016/j.ijthermalsci.2011.03.011
[23] J. Niu and Z. Zhu, "Numerical study of three-dimensional flows around two identical square cylinders in staggered arrangements," Phys Fluids, vol. 18, no. 4, 2006. https://doi.org/10.1063/1.2194077
[24] J. Aboueian and A. Sohankar, "Identification of flow regimes around two staggered square cylinders by a numerical study," Theor Comput Fluid Dyn, vol. 31, pp. 295-315, 2017. https://doi.org/10.1007/s00162-017-0424-2
[25] H. Rahman, S. Islam, W. Abbasi, and G. Nazeer, "A numerical study for flow around three square cylinders in triangular arrangement," Iranian J Sci Technology, Tran Mec Eng, vol. 44, pp. 229-246, 2020. https://doi.org/10.1007/s40997-019-00283-2
[26] W. Zhang, X. Chen, H. Yang, H. Liang, and Y. Wei, "Forced convection for flow across two tandem cylinders with rounded corners in a channel," Int J Heat Mass Transf, vol. 130, pp. 1053-1069, 2019. https://doi.org/10.1016/j.ijheatmasstransfer.2018.10.125
[27] N. Mahir and Z. Altaç, "Numerical investigation of flow and heat transfer characteristics of two tandem circular cylinders of different diameters," Heat Tran Engi, vol. 38, no. 16, pp. 1367-1381, 2017. https://doi.org/10.1080/01457632.2016.1255027
[28] Y. Gao, W. Chen, B. Wang, and L. Wang, "Numerical simulation of the flow past six-circular cylinders in rectangular configurations," J Mar Sci Technol, vol. 25, pp. 718-742, 2020. https://doi.org/:10.1007/s00773-019-00676-7
[29] J.-J. Yin, T. Jia, D. Gao, and F. Xiao, "Numerical investigation of the patterns of the flow past nine cylinders at low Reynolds number," AIP Adv, vol. 10, no. 8, 2020. https://doi.org/10.1063/5.0015541
[30] N. Hosseini, M. Griffith, and J. Leontini, "The flow past large numbers of cylinders in tandem," J Fluids Struct, vol. 98, p. 103103, 2020. https://doi.org/10.1016/j.jfluidstructs.2020.103103
[31] W. Zhang, H. Yang, H.-S. Dou, and Z. Zhu, "Forced convection of flow past two tandem rectangular cylinders in a channel," Numeri Heat Transf A Appl, vol. 72, no. 1, pp. 89-106, 2017. https://doi.org/10.1080/10407782.2017.1353384
[32] A. Sohankar, M. Khodadadi, E. Rangraz, and M. M. Alam, "Control of flow and heat transfer over two inline square cylinders," Phys Fluids, vol. 31, no. 12, 2019. https://doi.org/10.1063/1.5128751